THE JOURNAL OF PHYSICAL CHEMISTRY C

Article

Cite This: J. Phys. Chem. C 2019, 123, 28867−28880

pubs.acs.org/JPCC

Extended Discrete Interaction Model: Plasmonic Excitations of Silver Nanoparticles

Vadim I. Zakomirnyi,[†,‡,§] Zilvinas Rinkevicius,[†,∥] Glib V. Baryshnikov,[†] Lasse K. Sørensen,[†] and Hans Ågren*[,‡,†,⊥]

[†]Department of Theoretical Chemistry and Biology, School of Engineering Sciences in Chemistry, Biotechnology and Health, Royal Institute of Technology, Stockholm SE-10691, Sweden

[‡]Federal Siberian Research Clinical Centre under FMBA of Russia, Kolomenskaya 26, Krasnoyarsk 660037, Russia

[§]Kirensky Institute of Physics, Federal Research Center KSC SB RAS, Krasnoyarsk 660036, Russia

[∥]Department of Physics, Kaunas University of Technology, Kaunas LT-51368, Lithuania

[⊥]College of Chemistry and Chemical Engineering, Henan University, Kaifeng 475004, Henan, P. R. China

ABSTRACT: We present a new atomistic model for plasmonic excitations and optical properties of metallic nanoparticles, which collectively describes their complete response in terms of fluctuating dipoles and charges that depend on the local environment and on the morphology of the composite nanoparticles. Being atomically dependent, the total optical properties, the complex polarizability, and the plasmonic excitation of a cluster refer to the detailed composition and geometric characteristics of the cluster, making it possible to explore the role of the material, alloy mixing, size, form shape, aspect ratios, and other geometric factors down to the atomic level and making it useful for the design of plasmonic particles with particular strength and field distribution. The model is parameterized from experimental data and, at present, practically implementable for particles up to more than 10 nm (for nanorods even more), thus covering a significant part of the gap between the scales where pure quantum calculations are possible and where pure classical models based on the bulk dielectric constant apply. We utilized the method to both spherical and cubical clusters along with nanorods where we demonstrate both the size, shape, and ratio dependence of plasmonic excitations and connect this to the geometry of the nanoparticles using the plasmon length.

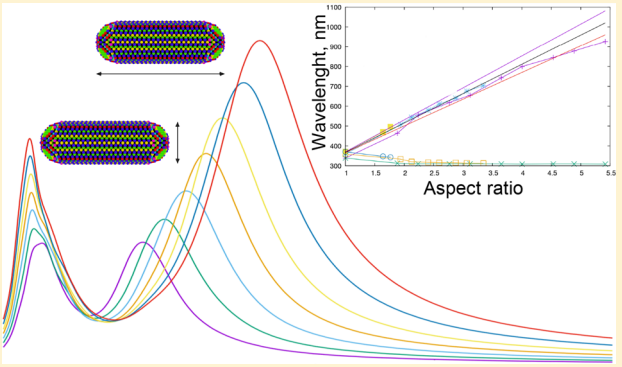

INTRODUCTION

Plasmonic excitations of metal elements can generate very strong electric fields in their vicinity through the interaction with electromagnetic radiation, leading to the possibility to detect signals of single molecules. There is a delicate requirement for matching the frequency of the incident light with that of the oscillating surface electrons, which depends ultimately on electronic structure and indirectly also on the size, shape, and material of nanostructured particles. It still remains a great challenge to design active plasmonic nanomaterials with arbitrary size, composition, and structure where the structures have the dimension of a few nanometers. Classical electrodynamics methods serve in general as viable approaches for prediction of the optical properties, including plasmonic generation[1−3] for larger particles where a variety of approaches, including the finite difference time domain (FDTD) method[4,5] and the finite element method (FEM),[6] frequently have been used for both time- and frequency-domain calculations. Furthermore, Mie theory[1] is frequently used for scattering problems involving nanoparticles that are sufficiently large proving that the concept of a classical dielectric constant remains valid. Other classical electrodynamics methods, such as the discrete dipole approximation[2] and the T-matrix method,[3] have also been widely used for calculation of optical properties of nanospheres, nanodisks, nanorods, and other complex geometrical configurations. The efficiency of these methods has been confirmed many times, and nevertheless, they tend to lose accuracy for small particles with a diameter below 10 nm. Corrections for these models that take into account quantum size effects[7] improve the results;[8,9] however, they still use dielectric constants of bulk materials, obtained empirically,[10] and do not consider the discrete atomic structure of the nanoparticles. It is thus obvious that the dielectric constant will vary in size and become unpredictable for small clusters with broad plasmon resonances or for clusters with more complex shapes. Here, the

Received: August 3, 2019
Revised: September 24, 2019
Published: October 16, 2019

Downloaded via STATE PUBLIC SCI TECHN LIB on July 15, 2020 at 12:20:04 (UTC).
See https://pubs.acs.org/sharingguidelines for options on how to legitimately share published articles.

© 2019 American Chemical Society

DOI: 10.1021/acs.jpcc.9b07410
J. Phys. Chem. C 2019, 123, 28867−28880

particle size can be smaller than the mean free path of the conduction electrons, and the surface to volume ratio can become so large that a significant deviation from a nonlocal bulk-value description of the dielectric constant can be expected. It is clear that there is a breaking point in size where quantum mechanics-based descriptions, accounting also for electronic structure, are necessary and where classical electrodynamics becomes too crude. Full quantum methods, such as the time-dependent density functional theory (TDDFT), can be useful for calculating the absorption spectra of a small cluster of noble metals with the number of atoms $N \approx 10-300$ using TDDFT when the cluster displays some higher symmetry.[11−16] However, due to obvious scaling limitations, such calculations cannot be performed for a large number of atoms.

For calculations of optical properties of intermediate-sized particles with 10^2-10^5 atoms and a diameter of a particle of $d < 10$ nm, an atomistic approach where the polarizabilities can be obtained from the atoms of the particle could fill an important gap in the description of nanoparticle plasmons between the quantum and classical extremes. Here, the classical dipole approximation can be applicable to construct the total polarizability (or the dielectric constant) from a set of interacting complex polarizable atomic dipoles. However, still for the polarizabilities as such, fixed constants are typically used for each type of element, obtained either from bulk measurements or electronic structure calculations. This neglects, for example, any charge rearrangement that takes place in the real cluster on formation or by molecular sensitization. An elaborate model yet very simple compared to quantum chemical calculations to deal with this is the so-called interaction model.[17] In the simplest form, it is a set of atomic polarizabilities that interact in accordance with classical electrostatics without an external electric field. One of the significant drawbacks of an interaction model is, however, that the atoms on the surface and inside of the cluster do not differ very much. The model has been significantly expanded by inclusion of a damping term of the internal electric field[18,19] and has been extended also to compute for the frequency dependence of the dipole polarizability[20,21] and to an atomistic discrete interaction model (DIM).[22,23] The discrete interaction models have been successfully applied to study the polarizability of organic molecules and metallic clusters, to model electrostatic interactions in molecular dynamics simulations, and to describe a heterogeneous environment in hybrid quantum mechanics/classical mechanics calculations; see, for example, ref 23. However, despite the atomistic nature, the DIM has limited capabilities to describe the dependence of the polarizability of the surface topology of the metallic nanoparticles, and furthermore, it cannot be used to study the polarizability of composite nanoparticles. Recently, Chen et al.[24] developed a coordination-dependent discrete interaction model (cd-DIM), which attempts to overcome these limitations of the original DIM. The new cd-DIM has been successfully applied to study optical properties of ligand-coated silver nanoparticles. Here, we propose an extended discrete interaction model (ex-DIM), which goes beyond the cd-DIM and enables a robust description of the polarizability of nanoparticles with different geometries. In the following theory section, we will describe our new extended discrete interaction method and compare it with the discrete interaction model and coordination-dependent discrete interaction model by Jensen et al.[22,25] and Chen et al.,[24] respectively, emphasizing the strengths and weaknesses of the models. We then discuss a different parameterization scheme based on experimental results and not on TDDFT as has otherwise been done with similar atomistic models. The interplay of parameters and how these parameters should be optimized and chosen are also discussed.

We demonstrate the size, shape, and aspect ratio dependence of surface plasmon resonances (SPRs) for silver spherical and cubical clusters and nanorods. We, here, theoretically and numerically show the inverse proportionality between the plasmon length and the SPR and not direct proportionality as proposed by Ringe et al.[26] Furthermore, we show that, for nanorods with the same diameter, the longitudinal localized surface plasmon resonance (LLSPR) and transverse localized surface plasmon resonance (TLSPR), measured in nanometers, are proportional to the aspect ratio and red and blue shifts, respectively. Furthermore, we show that the slope of the SPRs depends on the diameter of the nanorod and the polarizability per atom increases linearly with the aspect ratio in nanorods. Finally, we conclude and give an outlook of future developments and applications.

THEORY

We split the description of our extended discrete interaction model into two parts: a theoretical foundation and detailed description of the ex-DIM presented in this section and a parameterization scheme of the ex-DIM along with applications in the following section.

Extended Discrete Interaction Model. Similar to the original DIM suggested by Jensen et al.,[20,22] our extended discrete interaction model aims to describe the polarizability and optical properties of metallic nanoparticles by representing the nanoparticle as a collection of interacting atomistic charges and dipoles. The starting point of both models is a Lagrangian function with an energy expression for interacting fluctuating charges and dipoles in an external electric field subject to a charge equilibration constraint.

$$
\begin{aligned}
L[\{\mu, q\},\lambda] &= E[\{\mu, q\}] - \lambda\left(q^{\mathrm{tot}} - \sum_i^N q_i\right) \\
&= \frac{1}{2}\sum_i^N q_i \mathbf{c}_{ii}^{-1} q_i + \frac{1}{2}\sum_i^N \sum_{j\neq i}^N q_i \mathbf{T}_{ij}^{(0)} q_j \\
&\quad + \frac{1}{2}\sum_i^N \mu_i \boldsymbol{\alpha}_{ii}^{-1} \mu_i - \frac{1}{2}\sum_i^N \sum_{j\neq i}^N \mu_i \mathbf{T}_{ij}^{(2)} \mu_j \\
&\quad - \sum_i^N \sum_{j\neq i}^N \mu_i \mathbf{T}_{ij}^{(1)} q_j + \sum_i^N q_i \mathbf{V}^{\mathrm{ext}} \\
&\quad - \sum_i^N \mu_i \mathbf{E}^{\mathrm{ext}} - \lambda\left(q^{\mathrm{tot}} - \sum_i^N q_i\right)
\end{aligned} \tag{1}
$$

In eq 1, the first term is the self-interaction energy of fluctuating charges, the second term is the interaction energy between fluctuating charges, the third term is the self-interaction energy of fluctuating dipoles, the fourth term is the interaction energy between fluctuating charges and dipoles, the fifth term is the interaction energy between fluctuating dipoles, the sixth term is the interaction energy between fluctuating charges and the external potential, the seventh term is the interaction energy between fluctuating dipoles and the

DOI: 10.1021/acs.jpcc.9b07410
J. Phys. Chem. C 2019, 123, 28867−28880

external field, and the last term is a charge equilibration condition expressed via the Lagrangian multiplier λ. Here, q_i is the fluctuating charge assigned to the ith atom, μ_i is the fluctuating dipole assigned to the ith atom, $\mathbf{c}_{ii}$ is the ith charge self-interaction tensor, $\boldsymbol{\alpha}_{ii}$ is the ith dipole self-interaction tensor, $\mathbf{T}_{ij}^{(0)}$, $\mathbf{T}_{ij}^{(1)}$, and $\mathbf{T}_{ij}^{(2)}$ are the electrostatic interaction tensors, $\mathbf{V}^{\text{ext}}$ is the external potential, the $\mathbf{E}^{\text{ext}}$ is the external electric field, q^{tot} is the total charge of the nanoparticle, and N is the number of atoms in a nanoparticle. $\mathbf{T}_{ij}^{(0)}$, $\mathbf{T}_{ij}^{(1)}$, and $\mathbf{T}_{ij}^{(2)}$ are for the ex-DIM, shown in more detail in Appendix A. The fluctuating charges and dipoles are determined by minimizing the energy $E[\{\mu, q\}]$. According to Jensen et al.,[22] this minimization problem can be recast into a problem of solving a set of linear equations

$$\begin{pmatrix} \mathbf{A} & -\mathbf{M} & 0 \\ -\mathbf{M}^{\mathrm{T}} & -\mathbf{C} & 1 \\ 0 & 1 & 0 \end{pmatrix} \begin{pmatrix} \mu \\ \mathbf{q} \\ \lambda \end{pmatrix} = \begin{pmatrix} \mathbf{E}^{\text{ext}} \\ \mathbf{V}^{\text{ext}} \\ q^{tot} \end{pmatrix} \tag{2}$$

where the column vector μ is the collection of μ_i dipoles, the column vector $\mathbf{q}$ is the collection of q_i charges, and λ is a Lagrangian multiplier associated with charge equilibration condition. The matrix elements of $\mathbf{A}$, $\mathbf{C}$, and $\mathbf{M}$ are defined as

$$\begin{aligned} \mathbf{A}_{ij} &= \delta_{ij}\boldsymbol{\alpha}_{ij}{}^{-1} - (1-\delta_{ij})\mathbf{T}_{ij}^{(2)} \\ \mathbf{C}_{ij} &= \delta_{ij}\mathbf{c}_{ii}{}^{-1} + (1-\delta_{ij})\mathbf{T}_{ij}^{(0)} \\ \mathbf{M}_{ij} &= (1-\delta_{ij})\mathbf{T}_{ij}^{(1)} \end{aligned} \tag{3}$$

Equation 2 can be solved by inversion of the left-hand side matrix for small- and medium-size nanoparticles or by the iterative approach, such as the conjugate gradient method for large-size nanoparticles in an external field and potential. In the calculations presented here, we solve the linear equations by inversion for each frequency since we do not apply an external field. After that, the fluctuating charges and dipoles determined by the polarizability of the nanoparticle can be directly obtained by computing the second derivative of $E[\{\mu, q\}]$ with respect to external field $\mathbf{E}^{\text{ext}}$. According to Jensen et al.,[22,24] the polarizability of a nanoparticle can be defined as

$$\boldsymbol{\alpha}^{\text{np}} = \sum_{i}^{N} \frac{\partial \mu_i}{\partial \mathbf{E}^{\text{ext}}} \tag{4}$$

The above-described scheme for determination of the polarizability of a nanoparticle is generic and has been employed in the original, coordination-dependent, and extended discrete interaction models.[18−21,27,28] The differences between these models originate from the functional form used to describe the fluctuating charges and dipoles and from the parameterization of the self-interaction and electrostatic interaction tensors. To lay the foundation for our extended discrete interaction model, we first consider the parameterization of the DIM and cd-DIM. In the original DIM, the self-interaction tensors ($\mathbf{c}_{ii}$ and $\boldsymbol{\alpha}_{ii}$) are parameterized using atomistic capacitance and polarizability derived from bulk-material properties, and the electrostatic interaction tensors ($\mathbf{T}_{ij}^{(0)}$, $\mathbf{T}_{ij}^{(1)}$, and $\mathbf{T}_{ij}^{(2)}$) are computed using normalized Gaussian charges and dipoles with parameterization using TDDFT. In the cd-DIM, the fluctuating charges are excluded from the energy expression $E[\{\mu, q\}]$, the self-interaction tensor ($\boldsymbol{\alpha}_{ii}$) between dipoles is parameterized using a coordination number-dependent atomistic polarizability derived via the Clausius−Mossotti relation,[29] and the electrostatic interaction tensor ($\mathbf{T}_{ij}^{(2)}$) is computed by the same way as in the DIM. In order to extend these models and achieve a description of more complex surface topologies, we spatially spread in our model the Gaussian dipoles and charges in a way that they explicitly depend on their local chemical environment. Here, suggestively, the scheme of Grimme,[11] originally proposed for the computation of dispersion corrections in DFT calculations, can be used for evaluating atomic coordination numbers. The atomic coordination number f_{cn}^i is then computed as

$$f_{\text{cn}}^i = \sum_{i}^{N}\sum_{j\neq i}^{N} [1 + e^{-k_1(k_2(R_i^{\text{cov}}+R_j^{\text{cov}})/r_{ij}-1)}]^{-1} \tag{5}$$

where R_i^{cov} and R_j^{cov} are the scaled covalent radius of the ith and jth atoms, respectively, r_{ij} is the distance between the ith and jth atoms, and k_1 and k_2 are empirical parameters equal to 16.0 and 4.0/3.0, respectively.[30] In the case of fluctuating charges and dipoles, the normalized Gaussian charge distribution

$$G(\mathbf{r};\, \mathbf{C}) = \left(\frac{a}{\pi}\right)^{3/2} \exp[-a(\mathbf{r}-\mathbf{C})^2] \tag{6}$$

used in the DIM and cd-DIM can be replaced with the coordination number-dependent Gaussian charge distribution

$$\begin{aligned} G(\mathbf{r};\, f_{\text{cn}},\, \mathbf{C}) &= \left(\frac{a_{\text{cn}}}{\pi}\right)^{3/2} \exp[-a_{\text{cn}}(\mathbf{r}-\mathbf{C})^2] \text{ with } a_{\text{cn}} \\ &= a(1 + bf_{\text{cn}}) \end{aligned} \tag{7}$$

The coordination number-dependent dipoles are obtained from coordination-dependent Gaussian charges by taking their gradient, that is, $\mu(\mathbf{r};\, f_{\text{cn}},\, \mathbf{C}) = -\nabla_{\mathbf{r}} G(\mathbf{r};\, f_{\text{cn}},\, \mathbf{C})$. Here, a is the fixed exponent of the Gaussian charge distribution centered on the atom with the position vector $\mathbf{C}$, and b is the coordination number scaling factor, which defines the coordination number-dependent spread of the Gaussian charge distribution.

This constitutes the general form of the extended DIM. However, before taking on its full implementation, it is necessary to scrutinize the calculation of its most important parameters, namely, the self-interaction tensors $\mathbf{c}_{ii}$ and $\boldsymbol{\alpha}_{ii}$. Here, we adopt a scheme based on the concept of plasmon length[26] as described in the section below.

Modeling Capacitance and Polarizability. The parameterization of the self-interaction tensors, $\mathbf{c}_{ii}$ and $\boldsymbol{\alpha}_{ii}$, in the ex-DIM is central since these tensors play the dominant role in defining the behavior of the nanoparticle polarizability. Furthermore, in the case of dynamic polarizabilities, the frequency dependence is solely defined by these tensors. Similar to the DIM and cd-DIM, we use in the ex-DIM a diagonal isotropic form for the self-interaction tensors, that is, $\mathbf{c}_{ii,\,kl} = \delta_{kl}c$ and $\boldsymbol{\alpha}_{ii,\,kl} = \delta_{kl}\alpha$ for $k, l = x, y, z$. Here, we will employ a different strategy based on the plasmon length[26] to parameterize the $\mathbf{c}_{ii}$ and $\boldsymbol{\alpha}_{ii}$ tensors.

Starting from the self-interaction tensor via the Clausius−Mossotti relationship for a spherical particle

$$\boldsymbol{\alpha}_{ii,kl}(\omega) = \delta_{kl} f_\alpha \text{ with } f_\alpha = \frac{6}{\pi} R_i{}^3 \frac{\varepsilon(\omega) - \varepsilon_0}{\varepsilon(\omega) + 2\varepsilon_0} \tag{8}$$

where R_i is the radius of the ith atom, $\varepsilon(\omega)$ is the frequency-dependent dielectric constant of the material, and ε_0 is the

DOI: 10.1021/acs.jpcc.9b07410
J. Phys. Chem. C 2019, 123, 28867−28880

dielectric constant of the environment. In the DIM,[25] eq 8 is approximated as

$$\boldsymbol{\alpha}_{ii,kl}(\omega = 0) = \boldsymbol{\alpha}_{i,s,kl} \tag{9}$$

$$\boldsymbol{\alpha}_{ii,kl}(\omega > 0) = \boldsymbol{\alpha}_{i,s,kl}(L_1(\omega) + L_2(\omega, N)) \tag{10}$$

where $\boldsymbol{\alpha}_{i,\,s,\,kl}$ is the static polarizability and $L_1(\omega)$ and $L_2(\omega, N)$ are two separately normalized frequency-dependent Lorentzian functions. The resonance frequency $\omega_{i,2}(N)$ in $L_2(\omega, N)$ is size-dependent

$$\omega_{i,2}(N) = \omega_{i,2}(1 + A/N^{1/3}) \tag{11}$$

where N is the number of particles and $\omega_{i,2}$ and A are two fitted parameters. In this way, the size-dependent frequency is inversely proportional to the radius for spherical particles. The problems here are the discontinuity going from the static to the dynamic case due to the separately normalized Lorentzian functions and that the size-dependent resonance frequency in $L_2(\omega, N)$ does not take into account the geometry of the particle.

The cd-DIM[24] modifies the radius of eq 8 to a coordination number-dependent radius $R_i(f_{cn})$ and dielectric constant $\varepsilon(\omega, f_{cn}, r)$

$$\boldsymbol{\alpha}_{ii,kl}(\omega) = \delta_{kl} f_\alpha \text{ with } f_\alpha = \frac{6}{\pi} R_i{}^3(f_{cn}) \frac{\varepsilon(\omega, f_{cn}, r) - \varepsilon_0}{\varepsilon(\omega, f_{cn}, r) + 2\varepsilon_0} \tag{12}$$

Here, $\varepsilon(\omega, f_{cn}, r)$ is described by the sum of the experimental dielectric constant ε_{exp} and the size-dependent Drude equation minus the Drude function for spherical particles

$$\varepsilon(\omega, f_{cn}, r) = \varepsilon_{exp} + \varepsilon^{size}_{Drude}(\omega, f_{cn}, r) - \varepsilon_{Drude}(\omega) \tag{13}$$

where the plasma frequency in the size-dependent Drude function is modified by the coordination number. By using an effective coordination number, there is a smooth transition from the inside to the outside of the coordination sphere.

Both the DIM and cd-DIM should be able to describe the size dependence of spherical and sphere-like particles if properly parameterized. For shapes far from a spherical symmetry, such as nanorods with a large aspect ratio, the functional shape in the DIM and cd-DIM does not appear to be appropriate. We are therefore interested in developing a method that can take into account both the surface effects and geometry effects of nanoclusters.

We here extend the DIM where

$$\boldsymbol{\alpha}_{ii,kl}(\omega) = \left(\frac{R_i(f_{cn})}{R_{i,bulk}}\right)^3 \boldsymbol{\alpha}_{i,s,kl} L(\omega, \mathbf{P}) \tag{14}$$

is the static polarizabilty $\boldsymbol{\alpha}_{i,\,s,\,kl}$[31] multiplied by a normalized Lorentzian function of $L(\omega, \mathbf{P})$ and the relative shift in radius from the bulk radius is determined by the coordination number. In this parameterization scheme, the chemical environment enters the definition of the $\boldsymbol{\alpha}_{ii}$ tensor via $R_i(f_{cn})$ defined as

$$R_i(f_{cn}) = r_1\left(1 - \frac{f_{cn}}{12}\right) + r_2\frac{f_{cn}}{12} \tag{15}$$

which regulates the radii of the atom depending on the coordination number. For Ag, we use r_1 = 1.65 Å and r_2 = $R_{i,\,bulk}$ = 1.56 Å, which are the surface and bulk radii, respectively.[24] $L(\omega, \mathbf{P})$ regulates the geometric dependence via the size-dependent resonance frequencies of three size-dependent Lorentzian oscillators

$$L(\omega, \mathbf{P}) = N(L_x(\omega, P_x) + L_y(\omega, P_y) + L_z(\omega, P_z)) \tag{16}$$

where each $L_i(\omega, P_i)$ depends on the plasmon length P_i in the ith direction and the frequency ω with the common normalization factor N ensuring that the Lorentzian oscillators are normalized in the static limit of ω = 0. With a size-dependent Lorentzian oscillator in each direction, it is possible to describe more complicated geometric structures with multiple plasmon resonances without having a new functional dependence for each distinct geometry and thereby make the ex-DIM more universal. The Lorentzian oscillator is chosen as

$$L_i = \frac{1}{\omega_i{}^2(P_i) - \omega^2 - i\gamma\omega} \tag{17}$$

where γ describes the broadening of the spectra and $\omega_i(P_i)$ is the size-dependent resonance frequency, which enables the geometric description of the plasmon excitations. With the choice of the Lorentzian oscillator in eq 17, the normalization constant becomes

$$N = \left(\frac{1}{\omega_x{}^2(P_x)} + \frac{1}{\omega_y{}^2(P_y)} + \frac{1}{\omega_z{}^2(P_z)}\right)^{-1} \tag{18}$$

The choice of the Lorentzian oscillator in eq 17 and the common normalization in eq 18 will in this way give the higher peak for the lower incident frequency, which, for nanorods, corresponds to the long side. The size-dependent resonance frequency $\omega_i(P_i)$ can be written as

$$\omega_i(P_i) = \omega_a(1 + A{\cdot}f(N, i)) \tag{19}$$

where ω_a and A are atom-specific fitted parameters for the bulk resonance and size dependence, while $f(N, i)$ is a function of the number of atoms and dimension along the ith direction measured in units of atom i. $f(N, i)$ must then in the bulk and atomic limits fulfill

$$\lim_{N,i\to\infty} f(N, i) = 0 \quad \lim_{N,i\to 1} f(N, i) = 1 \tag{20}$$

which can easily be accomplished using a single parameter, namely, the plasmon length P_i

$$f(N, i) = \frac{1}{P_i} \tag{21}$$

where the plasmon length P_i is defined as the maximum distance between any atoms along the ith direction plus the radius of each of the endpoint atoms. This use of the plasmon length is consistent with the experimental work from Tiggesbäumker et al.[32] We here notice that the SPR cannot be directly proportional to the plasmon length as defined by Ringe et al.[26] since, in the bulk limit, the SPR would incline to minus infinity. Performing a Taylor expansion of eq 21, the first order is linear in the plasmon length, and therefore the linear dependence on the plasmon length as observed by Ringe et al.[26] is consistent with a sample of clusters of a limited size range. For spherical clusters, eq 21 reduces to the usual size dependence for classical models, also seen in the DIM and cd-DIM, but for rods, discs, and other shapes far from spherical, there is a distinct difference where the ex-DIM can have up to three distinct plasmon resonances.

DOI: 10.1021/acs.jpcc.9b07410
J. Phys. Chem. C 2019, 123, 28867−28880

The $\mathbf{c}_{ii}$ tensor responsible for the self-interaction energy in charge transfer processes is in the DIM modeled as

$$c_i(\omega) = c_{i,s} L_1(\omega) \tag{22}$$

using the same size-independent Lorentzian function as in eq 10 for the polarizability in the DIM and a fitted parameter $c_{i,s}$ for the "static atomic capacitance". In the cd-DIM, the charges and hence the charge transfer and capacitance are completely removed.

In the ex-DIM, we adopt a simplified two-parameter parameterization scheme

$$c_{ii,kl} = \delta_{kl} f_c \text{ with } f_c = c_{i,s}\left[1 + d\frac{R_i(f_{cn})}{R_i(12)}\right] L(\omega, \mathbf{P}) \tag{23}$$

where c is the "static atomic capacitance" parameter, similar by its physical origin to the capacitance used in the DIM, d is a scaling factor for the coordination number dependence of the capacitance, set to 0.1, and $L(\omega, \mathbf{P})$ is the Lorentzian oscillator defined in eq 16. Here, we stress that, in our parameterization of the $\mathbf{c}_{ii}$ tensor, the frequency dependence is exactly the same as for the polarizability.

The outlined parameterization scheme of our ex-DIM not only satisfies the above given principal conditions for our model, physical limits, and geometric dependencies but also enables rapid reparameterization of the ex-DIM for new types of composite nanoparticles or/and their environments.

PARAMETERIZATION OF THE EXTENDED DISCRETE INTERACTION MODEL AND APPLICATIONS

Similar to its predecessors, the extended discrete interaction model is an empirical approach, and thus its accuracy and applicability are defined by the quality of its parameterization. Here, we outline the basic ideas behind the parameterization of the ex-DIM and discuss the optimization of the parameters for nanoparticles. As the ex-DIM aims to describe static and dynamic polarizabilities of metallic nanoparticles accurately, the goal of the parameterization is to obtain a set of parameters with which the SPRs are computed using eq 4 as close as possible to established benchmark values for a selected set of nanoparticles. We here optimize the model using a training set of spherical clusters and compare the results to both the experimental values and a validation set of larger clusters to ensure that the model gives reliable results for all cluster sizes. Afterward, we investigate if the redshift observed in the Au clusters by Ringe et al.[26] when going from more spherical clusters to cubical clusters also is present for Ag clusters. Finally, we turn our attention toward silver nanorods to show that both the longitudinal and transverse SPRs can be accurately predicted using the ex-DIM.

Parameterization of the ex-DIM Model. As discussed in detail in Appendix B, parameterizing the ex-DIM using TDDFT data from small silver clusters encounters problems with the magic number of atoms, limited size of clusters, and the more physical problem of not having real SPR. Therefore, trying to optimize the parameters minimizing the difference in the polarizability between a small set of clusters calculated using TDDFT and a given parameter range does not appear to be a viable approach. We have therefore instead opted to optimize the parameters in the ex-DIM directly from experimental results. For this, we have used the systematic size-dependence investigation of silver clusters performed by Scholl et al.[33] The aim therefore is not to reproduce the absolute polarizability of small TDDFT calculations but to predict the SPR of larger clusters with different geometry.

Even though there have been significant advances in geometry optimization of metal clusters, the problem still remains to be hard and not applicable for larger metal clusters due to a multitude of local minima close-lying in energy.[34−36] For all clusters and nanorods, we therefore start from a perfect lattice where all atoms have the same distance to their nearest neighbor and then cut out the nanoclusters with the desired structure. From the 310 Ag-atom cluster, the average distance to the closest neighbor is 5.28 au with a minimum and maximum distance of 5.17 and 5.41 au. Similar distances are seen for the other optimized clusters,[35] and we have therefore fixed the closest neighbor at 5.27 au in our lattice. Since the surface topologies of all measured nanoparticles with the same radius are slightly different, we try to capture this effect by having several clusters with the same plasmon length but a different number of particles in our optimization. This is possible since there are only small variations in the SPR with respect to small changes in the surface topology for sphere-like clusters. In the optimization, we do not use faceted clusters nor clusters with surface defects such as bumps or holes.

In order to reduce the number of parameters needed to be fitted and make the method easier to extend to other elements, we make use of experimental or theoretical literature values or make argued choices for parameters that affect the peak position of SPRs. The polarizabilities (α) are taken from Schwerdtfeger and Nagle,[31] which for silver are 55 au. The value of the capacitance parameter c, as shown in Appendix C, has very little influence on the overall polarizability and peak position as long as c is outside areas of numerical instability. For the optimization of sphere-like clusters, we have fixed the value at 0.0001 au since all systems appear to be numerically stable with this choice.

The Lorentzian broadening γ should be small compared to the incident frequency and, not surprisingly, should show no significant influence on the position of the SPR as seen in Appendix D. During optimization, γ has been fixed at 0.016 au, which gives what we deemed a reasonable broadening of the peak(s) with FWHM compared to that extrapolated from data by Ringe et al..[26] While the SPR(s) does not shift with γ except when two close-lying double peaks merge, the width and height of the SPR(s) are significantly influenced thereby making it difficult to get a good set of parameters when optimized together with α for a small set of small clusters. Despite being optimized with γ = 0.016, there is no problem adjusting this parameter later or making γ size-dependent to obtain different peak heights since the placement of the SPR(s) is not affected by small changes in γ.

The only parameters that need to be fitted are therefore the size-dependent resonance frequency ω_a and the size-dependence factor A. These two parameters are the decisive parameters in determining the SPR. Systematic investigations, like the one performed by Scholl et al.,[33] are therefore essential for an accurate fit of ω_a and A. Due to the scarce amount of data and because of what appear to be outliers in the data, we decided to perform some data pruning and base our parameter fit on the pruned data. By plotting the energy of the SPR as a function of the inverse plasmon length, we can fit a simple linear function as shown in Figure 1.

From the fit in Figure 1, the bulk limit for the SPR for Ag will be 3.25 eV in our model and will show a slow variation of

DOI: 10.1021/acs.jpcc.9b07410
J. Phys. Chem. C 2019, 123, 28867−28880

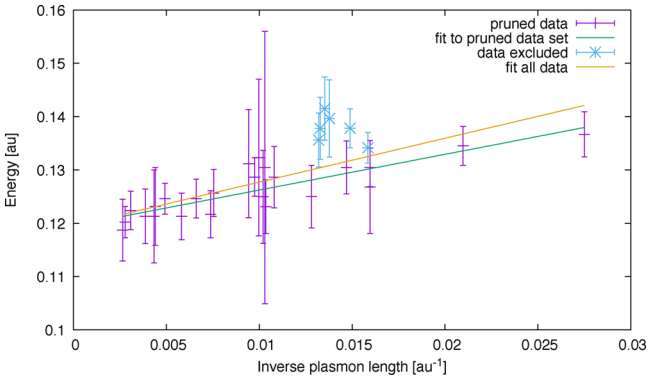

Figure 1. Linear fit $(ax + b)$ of experimental data with error bars from Scholl et al.[33] The purple points are the pruned data, and the green line is the fit of the pruned data with coefficients of a = 0.670796 ± 0.05917 and b = 0.119511 ± 0.0006792. The blue points are data excluded from the pruning, and the yellow-orange line is a fit of all data with coefficients of a = 0.822497 ± 0.1057 and b = 0.119488 ± 0.001297.

the SPR as a function of the inverse plasmon length. With the definition of the plasmon length in eq 21, the inverse plasmon length cannot exceed the inverse diameter of an atom, and the SPR is therefore finite.

By choosing a representative set of spherical clusters with a plasmon length of 1.4−3.8 nm, an optimal resonance frequency, $\omega_i P_i$ in eq 19, which exactly reproduces the SPR from the fit in Figure 1, for every cluster can be found (Figure 2). The optimal resonance frequency is here reproduced with a

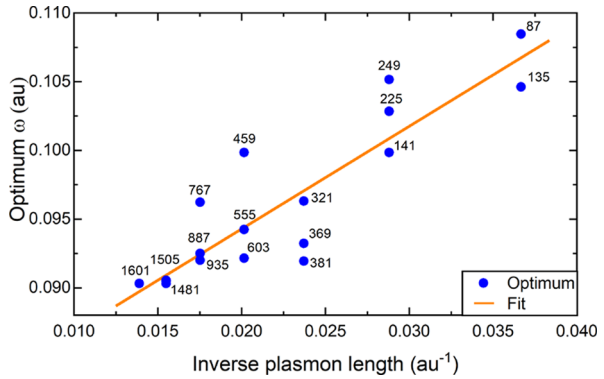

Figure 2. Optimum $\omega_i(P_i)$, which reproduces the plasmon peak at the fitted experimental values from Figure 1 for a given cluster. Fitting the optimum $\omega_i(P_i)$ to eq 19, we find that ω_a = 0.0794 au and A = 9.41 au. The 1409 and 1433 atom clusters, also included in the fit, are located between or underneath the 1481 and 1505 atom clusters.

deviation of 10^{-6}−10^{-5} of the SPR compared to experiments. We here use several spherical clusters with the same plasmon length but with different surface topologies to simulate slightly different surfaces. So while the radius in the 459, 555, and 603 clusters is the same, the number of atoms and the surface topology are not. We here find that ω_a = 0.0794 au and A = 9.41 au.

Inserting the fitted ω_a and A values and recalculating the clusters from the fit along with a test set of larger clusters with 276−11,849 atoms and a 2−7 nm diameter, we are able to reproduce the SPR from the fit of the experimental values as seen in Figure 3.

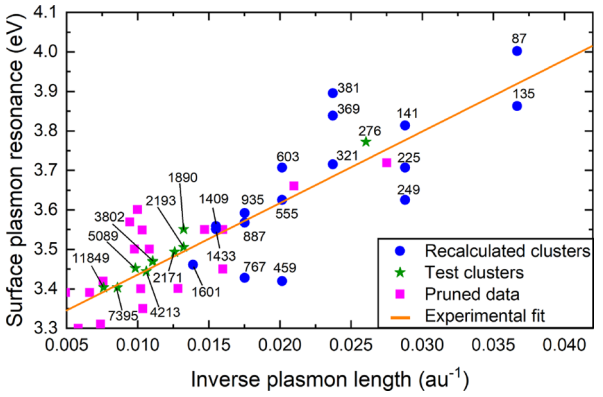

Figure 3. Plasmon peak as a function of the inverse plasmon length for the clusters used for the fit in Figure 2 and a test set with larger clusters calculated with the fitted ω_a and A values compared to the experimental fit and pruned data. The 1481 and 1505 atom recalculated clusters are located between or underneath the 1409 and 1433 atom clusters.

As seen from Figure 3, we are able to reproduce the SPR of any sphere-like cluster irrespective of size with an error limited by the experimental error. To ensure that the behavior of the polarizabilty is correct for all frequencies, we calculated the polarizability-dependent frequency for 200 points in the 3.0−4.6 eV region.

Comparison between the ex-DIM, DIM, and cd-DIM with Mie Theory. Since all three models have been applied to bare sphere-like silver clusters, it would be natural to compare them to the experimental data since the cd-DIM has been compared to the same data before[24] and the ex-DIM is parameterized from the experimental data. The extracted data from the DIM and cd-DIM have therefore been plotted against the experimental data and ex-DIM calculations as shown in Figure 4. From the plotted data, it is evident that, for the truncated octahedrons, the DIM shows no discernible trend, while for the icosahedra, there is a redshift of approximately 0.2 eV with size but only for the range of 147−1415 atoms (1.8−3.4 nm); thereafter, there is no shift. The cd-DIM does show a redshift in the plasmon length with increasing size but only by

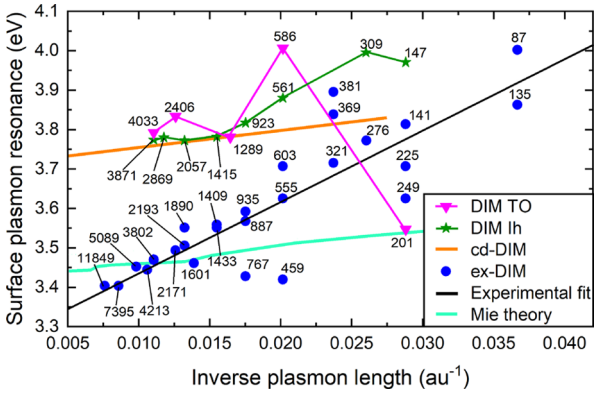

Figure 4. Comparison between the ex-DIM, DIM,[25] and cd-DIM,[24] Mie theory, and experiment for bare silver clusters.[33] For the DIM, the TO clusters are truncated octahedrons and Ih are icosahedral clusters. The diameter for the DIM clusters are estimated from the clusters used in the ex-DIM. The 1481 and 1505 atom recalculated clusters are located between or underneath the 1401 and 1433 atom clusters.

DOI: 10.1021/acs.jpcc.9b07410
J. Phys. Chem. C 2019, 123, 28867−28880

approximately 0.097 eV for the 2−10 nm clusters, while the experimental data give a redshift of 0.38 eV in that region. The limit of the cd-DIM therefore deviates significantly from the experimental results and the results of the ex-DIM. While Chen et al.[24] give an arbitrary shift of 0.2 eV to the experimental data to compensate for solvent effects, this does not change the fact that the shift in the SPR in the cd-DIM is only approximately a quarter of what it should be according to experiments.[33]

The poor performance of the DIM and cd-DIM for sphere-like clusters is most likely not due to methodological issues but rather due to the parameterization. This can be understood since the ex-DIM and DIM in the spherical cases are very similar except for the surface atoms, and a better fit of parameters should therefore be possible. For the DIM,[25] Jensen and Jensen reported puzzling parameters. While the resonance frequency $\omega_{i,1} = 0.0747$ is similar to $\omega_a = 0.0794$ in the ex-DIM, the broadening $\gamma_{i,1} = 0.0604$ is of the same size as the resonance frequency $\omega_{i,1}$, which is very unusual in Lorentzian and other oscillator models and a sign of something that has gone wrong in the parameterization. We here notice that Jensen and Jensen[22] use a capacitance parameter, $c = 3.45$, which is right in the region of numerical instability in the ex-DIM as shown in Appendix C. In cd-DIM, the size-dependent Drude function does not appear to be optimized for silver at all even though Karimi et al.[37] had no problems fitting a similar function for gold.

Mie theory[1] is known to be in good agreement with experiments for medium and large particles but not so for small particles. As seen in Figure 4, Mie theory underestimates the size dependence of small silver clusters when compared to experiments even when Mie theory is size-corrected based on the electron effective mean free path.[38]

Silver Cubes. Ringe et al.[26] showed that Au cubes are redshifted up to 0.2 eV in comparison to more sphere-like clusters with the same plasmon length. Because of differences in dielectric constants[39] between Au and Ag, the SPR in Ag nanoparticles has a more acute size dependence than that of their Au counterparts.[40,41] As seen from Figure 5, we predict that the more acute size dependence translates into a larger shape dependence of the SPR as the Ag cubes are redshifted at approximately 0.6 eV in comparison to the Ag spheres in the region examined here, which is in line with the findings of González et al.[42] The size dependence of the cubes and spheres is here shown to be reasonably similar.

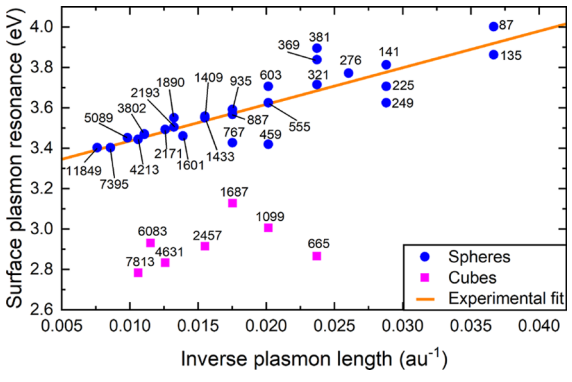

Figure 5. Comparison of the SPR for sphere and cubes with different plasmon lengths. The greater red and blue shifts seen for the 665 and 1687 atom cubical clusters, respectively, are due to double peaks where the most red- and blueshifted peaks have the highest polarizability. With a larger γ value, both outliers will be shifted to be more in line with the rest of the cubes. The 1481 and 1505 atom recalculated clusters are located between or underneath the 1401 and 1433 atom clusters.

Silver Nanorods. While a small red shift in the SPR with increasing cluster size is seen for sphere-like particles, very significant red shifts can be observed for nanorods depending on the aspect ratio. This very large red shift can be used to tune the SPR to a given region, thereby making nanorods versatile sensors. The SPR for nanorods is, however, split into two due to the cylindrical symmetry and excitation of collective oscillations of conduction electrons of nanorods, and two peaks are seen in the UV−vis spectrum. The SPR along the short transverse axis (TLSPR) is typically very slightly blueshifted in comparison to that of a spherical cluster with the same plasmon length, while the SPR along the long longitudinal axis (LLSPR) can be redshifted much below what can be done by increasing the size of a spherical cluster. Furthermore, the polarizability for the redshifted peak is also greatly enhanced with an increasing aspect ratio, here defined as the ratio between the plasmon length in the longitudinal and transverse directions.

Since tunable nanorods are of great application interest, we have examined a series of nanorods to elucidate the interplay between the aspect ratio and diameter with respect to the SPR. We have constructed a series of nanorods where each end is a half-sphere connected by a cylinder. The nanorods are designated as Ag(x, y) where x is the plasmon length of the longitudinal axis and y is the plasmon length of the transverse axis in nanometers as shown in Figure 6. Ag(y, y) is, with this

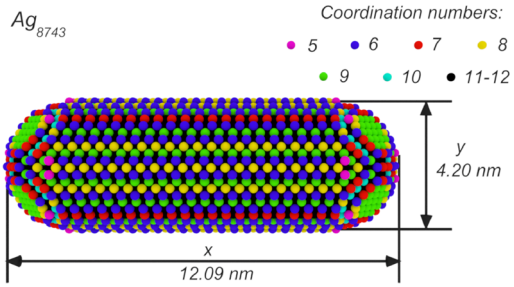

Figure 6. Longitudinal and transverse plasmon length and coordination numbers for the Ag(12.09, 4.20) nanorod, which contains 8743 atoms.

definition, a sphere with an effective diameter of y. We here use nanorods with a diameter from 2.23 to 6.18 nm, a length of up to 14.06 nm, and an aspect ratio of up to 5.4 and containing up to 16,567 atoms. For all figures, we calculate the polarizabilty at 400 different frequencies. In Figure 6, we clearly see that only the top layer of atoms has a coordination number below 11−12, and, as expected, the atoms with the lowest coordination number are on the edges. This means that only the surface atoms are directly affected by the changes introduced by the coordination numbers.

The red shift of the LLSPR for the Ag(x, 2.23) and Ag(x, 4.20) nanorods calculated with the ex-DIM is clearly visible from Figures 7 and 8. Due to the emergence of a double peak in Figure 7, the slight blue shift of the TLSPR is not as visible as in Figure 8. As seen in Figure 9, the red shift of the LLSPR in nanometers is directly proportional to the aspect ratio and the difference in the LLSPR changes with the diameter of the

DOI: 10.1021/acs.jpcc.9b07410
J. Phys. Chem. C 2019, 123, 28867−28880

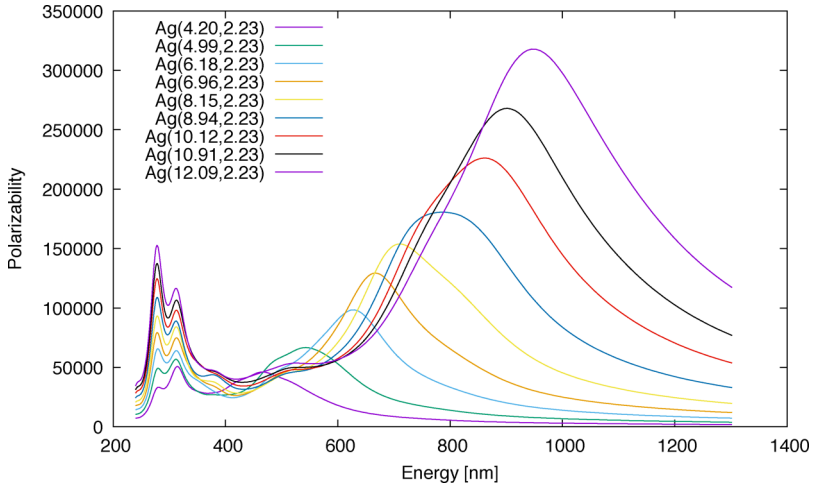

Figure 7. Polarizability as a function of the incident energy for Ag(x, 2.23) nanorods with different longitudinal plasmon lengths.

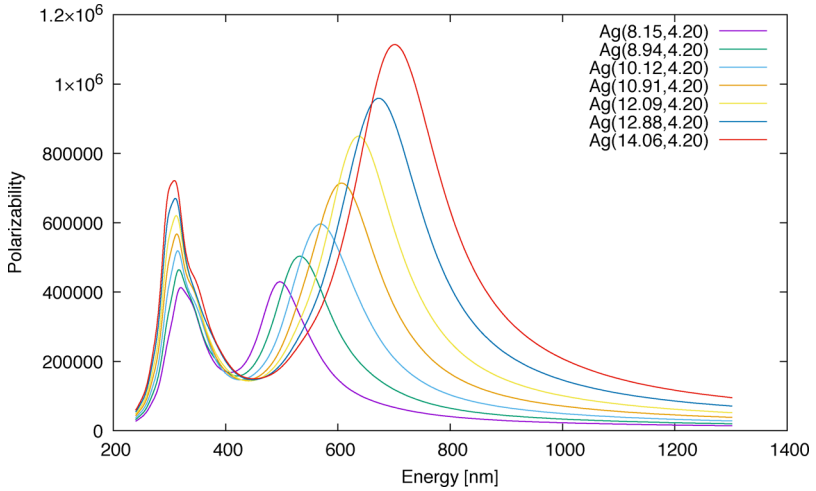

Figure 8. Polarizability as a function of the incident energy for Ag(x, 4.20) nanorods with different longitudinal plasmon lengths.

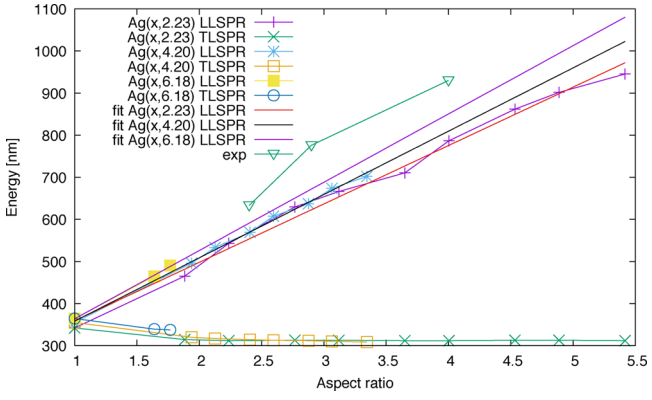

Figure 9. LLSPR, TLSPR, and fit of the LLSPR as a function of the aspect ratio for different nanorods. For the Ag(x, 2.23) nanorods, the TLSPR becomes a double peak (see Figure 7), and here, only the right TLSPR is included. These are compared to the experimental LLSPR in a 0.1 M KNO_3 aqueous solution.[45]

nanorod. The dependence on the diameter of the nanorod can also be seen from the slope of the fit for the Ag(x, 2.23), Ag(x, 4.20), and Ag(x, 6.18) nanorods, which are 139 ± 4, 150 ± 3, and 162 ± 7, respectively. The increasing slope of the LLSPR with the diameter is also observed for gold nanorods.[43,44] The slight blue shift of the TLSPR is best seen for the Ag(x, 4.20) and Ag(x, 6.18) nanorods and is also approximately linear. The experimental results of Jakab et al.[45] in which the average width of the nanorods varies from 55 to 59 nm indicate that the red shift is directly proportional to the aspect ratio and with a slight increase in the slope compared to our results. The large red shift in comparison to our results is due to the differences in the refractive index in the surrounding medium. Here, our results refer to nanorods on an ultrathin carbon film,[33] while the experimental results were obtained in a 0.1 M KNO_3 aqueous solution.

The relative polarizability and peak width between the LLSPR and TLSPR in Figures 7 and 8 are seen to increase significantly with an increasing aspect ratio. The polarizability per atom in Figure 10 is seen to increase linearly with the aspect ratio, and only minor changes are seen with respect to the diameter of the nanorod. Both the LLSPR and the absorbance can in this way be controlled by the aspect ratio and the diameter of the nanorods. The polarizability thus depends substantially on the geometry. For applications of nanorods, the refractive index of the surrounding medium must also be carefully considered.

DOI: 10.1021/acs.jpcc.9b07410
J. Phys. Chem. C 2019, 123, 28867−28880

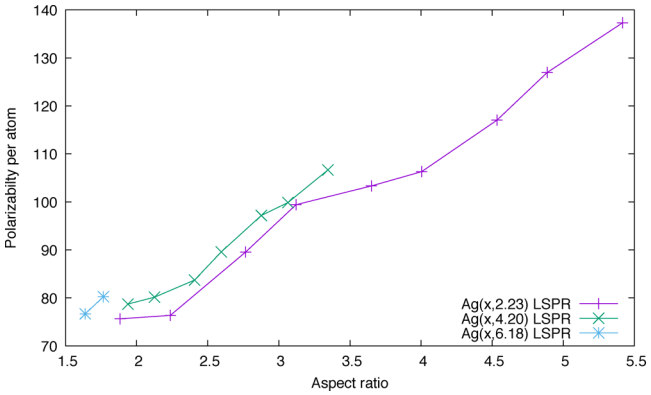

Figure 10. Polarizability per atom as a function of the aspect ratio.

OUTLOOK AND DISCUSSION

Motivated by the wide applicability of small plasmonic nanoparticles with a size between 1 and 15 nm and by the need to bridge this length gap between the classical and quantum theories to describe plasmon generation, we have presented in this work an extended discrete interaction model (ex-DIM) to simulate the geometric and environmental dependence of plasmons of this size. The frequency-dependent dielectric function is obtained from the Clausius−Mossotti relation as a sum of three Lorentzian oscillators and with Gaussian charge distributions and atomic radii that vary with the coordination number. The three frequency-dependent Lorentzian oscillators depend on the plasmon length in the *x*, *y*, and *z* directions with the plasmon length defined as in the work of Ringe et al.[26]

We here show both theoretically and numerically that the SPR is inversely proportional to the plasmon length and not proportional. We also show that, due to the limitations of applicable quantum calculations (N.B. TDDFT) and due to the interplay of parameters that fit an atomistic model for metal clusters, the use of absolute polarizabilities from TDDFT is not a viable approach. Instead, we show that the model can be parameterized from experiments[33] with a numerical accuracy of the same order as the experimental accuracy. Furthermore, we show that certain parameters such as the broadening and capacitance do not influence the peak position of the SPR to any appreciable extent and that reasonable values for these parameters can be chosen without fitting. We see almost no effect of the capacitance below a given value, while above that value, the system may become numerically unstable in contrast to some earlier work on fitting atomic capacitance parameters.

Having parameterized the model to a set of spherical clusters, we show that not only the training set but also the validation set with larger clusters are all very close to the experimental results unlike the DIM[22,25] and cd-DIM[24] results. To demonstrate the capabilities of the ex-DIM, we also performed a set of calculations on cubes and nanorods. For the cubes, we show that the SPR is redshifted in comparison to a spherical cluster with the same plasmon length, which is in line with the findings of González et al.[42] and the experimental findings of Ringe et al.[26] for Au clusters with the difference that the geometric dependence for Ag appears to be larger than that of Au. For the nanorods, we show a significant red shift for the longitudinal resonance and a very slight blue shift for the transverse resonance with the aspect ratio. By calculating several series of nanorods with different diameters and aspect radii, we show that the red shift is directly proportional to the aspect ratio and that the slope in all series of nanorods of different diameters shows a slight dependence on their plasmon length in the transverse direction similar to that seen for Au nanorods.[43,44] We compare these results to experiments and find that differences in the refractive index of the surroundings only appear to give a constant shift for the LLSPR.[45] Furthermore, we show that the polarizability per atom increases linearly with the aspect ratio, thereby making it possible to control both the peak position and the polarizability of the SPR for nanorods.

Our ex-DIM is flexible and versatile and brings wide ramifications, for instance, in the design of small plasmonic nanoparticles in mixed or alloyed systems with particular geometries in metal particle organic hybrids where the organic part receives comparable parameterization as the metal part in heterogeneous environments and in external fields. Work is ongoing to capitalize on these expectations.

APPENDIX A

Electrostatic Interaction Tensors

Similarly to the DIM and cd-DIM, our ex-DIM uses Gaussian electrostatics to describe the interaction of fluctuating charges and dipoles. However, in our model, normalized Gaussian charge distributions are explicitly dependent on the coordination number of the atom with which it is associated (see eq 7), and thus the electrostatic interaction tensors, $\mathbf{T}_{ij}^{(0)}$, $\mathbf{T}_{ij}^{(1)}$, and $\mathbf{T}_{ij}^{(2)}$, have more complex forms compared to the ones used in the DIM or cd-DIM. Assuming that we have two Gaussian charge distributions, $G(\mathbf{r}; f_{cn}, \mathbf{C})$ and $G(\mathbf{r}\,'; f'_{cn}, \mathbf{D})$ centered on the *i*th and *j*th atoms with position vectors **C** and **D**, the electrostatic interaction tensor $\mathbf{T}_{ij}^{(0)}$ between these charges can be computed as

$$\mathbf{T}_{ij}^{(0)} = \int\int \frac{G(\mathbf{r}; f_{cn}, \mathbf{C})G(\mathbf{r}'; f'_{cn}, \mathbf{D})}{|\mathbf{r} - \mathbf{r}'|}\mathrm{d}\mathbf{r}'\mathrm{d}\mathbf{r} = \frac{\mathrm{erf}(\gamma r_{ij})}{r_{ij}} \tag{24}$$

$$\gamma = \sqrt{\frac{a_{cn}a'_{cn}}{a_{cn} + a'_{cn}}} \text{ and } r_{ij} = |\mathbf{C} - \mathbf{D}| \tag{25}$$

Following Mayer,[46] the higher-order electrostatic interaction tensors, $\mathbf{T}_{ij}^{(1)}$ and $\mathbf{T}_{ij}^{(2)}$, can be obtained by taking the derivatives of $\mathbf{T}_{ij}^{(0)}$ with respect to the *i*th atom coordinates, that is

$$\mathbf{T}_{ij}^{(1)} = -\nabla_{\mathbf{r}_i}\mathbf{T}_{ij}^{(0)} = \frac{\mathbf{r}_{ij}}{\mathbf{r}_{ij}^{3}}\left[\mathrm{erf}(\gamma r_{ij}) - \frac{2\gamma r_{ij}}{\sqrt{\pi}}\exp(-\gamma^2 r_{ij}^{2})\right] \tag{26}$$

$$\begin{aligned}\mathbf{T}_{ij}^{(2)} &= -\nabla_{\mathbf{r}_i} \otimes \nabla_{\mathbf{r}_j}\mathbf{T}_{ij}^{(0)} \\ &= \frac{\mathbf{r}_{ij} \otimes \mathbf{r}_{ij} - r_{ij}^{2}\mathbf{I}}{r_{ij}^{5}}\left[\mathrm{erf}(\gamma r_{ij}) - \frac{2\gamma r_{ij}}{\sqrt{\pi}}\exp(-\gamma^2 r_{ij}^{2})\right] \\ &\quad - \frac{4\gamma^3\mathbf{r}_{ij} \otimes \mathbf{r}_{ij}}{\sqrt{\pi}\,r_{ij}^{2}}\exp(-\gamma^2 r_{ij}^{2})\end{aligned} \tag{27}$$

The above given expressions for interaction tensors can be easily reduced to the ones used in the DIM if one replaces the coordination number-dependent Gaussian exponents, a_{cn} and a'_{cn}, with appropriate effective radii (see eqs 11−13 in Jensen's work[22]).

DOI: 10.1021/acs.jpcc.9b07410
J. Phys. Chem. C 2019, 123, 28867−28880

APPENDIX B

Surface versus Bulk Plasmon Resonance in Small Silver Clusters

The accurate estimation of the electronic and spectral properties, such as static dipole polarizability, ionization potential, and electron affinity, and atomization energy and absorption and emission cross sections, is still a major challenge for small silver clusters.[15,47−49] The important property of silver clusters is that they can be considered at the same time as bulk metal particles and surface-active systems depending on the size of these species. Indeed, the electronic properties and spectra of small silver clusters (till 120 atoms that approximately correspond to the diameter of a spherical nanoparticle approximately 1.6 nm) are well described by the so-called shell model[50] that explains the strongly nonlinear behavior of these species with respect to the position of absorption maxima, static polarizability, ionization potential, and electron affinity parameters.[47,51] Particularly, it has been found that silver clusters with a magic number of atoms (8, 18, 34, 58, and 92) show a localized maximum value of the plasmon-like absorption energies at approximately 4.1 eV.[51,52] These numbers actually correspond to the fully filled states of 1s, 1p, 1d, 1f, 1g, and 1h electronic shells. Some previously published DFT calculations confirm such behavior[51,15] demonstrating that s valence electrons are distributed in delocalized orbitals in the following sequence of electronic shells: $1s^2$, $1p^6$, $1d^{10}$, $2s^2$, $1f^{14}$, $2p^6$,$1g^{18}$, $2d^{10}$, $3s^2$, $1h^{22}$, etc. It means that small silver clusters absorb light due to excitations of s electrons delocalized over the whole volume of the cluster, which explains that this band can be assigned as plasmon-like resonance or so-called bulk resonance, different from the commonly known SPR by a physical meaning. It is reasonable to suggest that the position of the bulk resonance should be weakly sensitive to the size and shape of the nanoparticle. Even for large silver nanoparticles, the bulk core (if we consider a cage model of the particle) still possesses similar localization and energy of s electrons as a small cluster, while the energy of the SPR expectantly depends significantly on the shape, curvature, type, and defects of the surface. Scholl et al.[33] clearly defined both types of resonances (bulk and surface) for spherical silver nanoparticles of the size of 2−23 nm from electron energy-loss spectroscopy by directing the electron beam to different zones of the particles from the edge through the bulk. Based on such focused excitation, surface and bulk resonances can be selectively observed in the range of 4.1−3.8 and 3.8−3.2 eV, respectively. One can see that the energy variation is more pronounced for the surface resonance, a tendency which is clearly size-dependent, while the bulk resonance is less size-dependent. The energy values are in a good agreement with our TDDFT/cam-B3LYP/Lanl2DZ[53−55] calculations for small metal clusters of Ag_n (n = 18−34) and with other previously published results.

An applicability of long-range corrected (LC) functionals for the correct simulation of optical transitions for small silver clusters in the gas phase was shown in few recent publications.[51,56] Particularly, LC hybrid functionals significantly reduce the occurrence of spurious states in the optical absorption spectra while maintaining the intensity of plasmon-like features of the spectra for larger silver clusters.[56]

The final spectra calculated using the long-range corrected cam-B3LYP functional for the nine Ag_n (n = 18−34) clusters (Figure 11, black curves) all exhibit an absorption peak at approximately 4 eV in good agreement with the experimental data for Ag_{18}, Ag_{20}, and Ag_{30} clusters (Figure 11, red curves).[52,57] For these three cases, the main computed absorption peak is blueshifted at approximately 0.2 eV relative to the experimental curves, which can be attributed to the matrix effect[16,51] (experimental spectra were measured for the clusters isolated in the noble gas matrix). Such a blue shift accords with that published in ref 51 (0.17 eV, estimated from direct comparison between the experimental spectra measured in a neon matrix at 6 K and TDDFT/ωB97x gas phase calculations). Visualization of Kohn−Sham molecular orbitals on Figure 12 responsible for the main most intensive electronic transition (black peaks under the spectral curves, Figure 11) clearly shows the delocalization of the valence and conductive s electrons mixed with the localized d functions over the whole volume of the studied clusters. It proves the "bulk" nature of the predicted resonance peak. Increasing of the cluster size greatly complicates the calculations of the bulk resonance position and its parameters because the number of excited states that lie lower than 4 eV significantly increases with the cluster that grows without additional symmetry constraints. For instance, for the Ag_{34} cluster, at least 250 excited states should be calculated for correctly reproducing the bulk plasmon resonance peak (here using Casida's transition-based approach).[58] One alternative way to solve this limitation and to simulate the optical absorption spectra of Ag clusters up to 561 atoms is a TDDFT time-evolution formalism proposed by Yabana et al.[59] and realized by Weissker et al. using the real-space code Octopus.[13,60,61] However, it does not principally solve the size limitation of TDDFT approximation with respect to silver clusters even using the less computationally expensive LDA approximation or applying symmetry constraints. Moreover, the small silver clusters are very unstable even in the presence of a coverage shell of organic ligands, something that complicates the investigation of their optical properties and

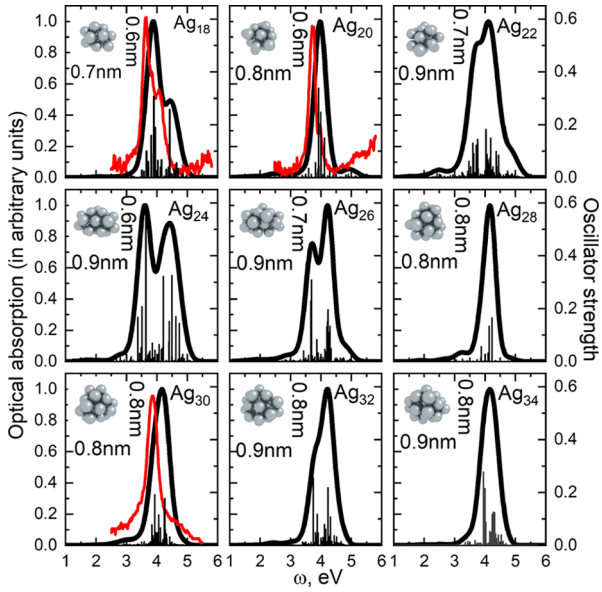

Figure 11. Absorption spectra of the Ag_n (n = 18−34) clusters calculated by the TDDFT/cam-B3LYP/Lanl2DZ method in the gas phase (black curves and black peaks correspond to the vertical electronic transitions) compared with experimental data (red curves were taken from refs 52 and 57). The Gaussian line shape with a full width at half maximum of 0.2 eV was used for the calculated spectra convolutions.

DOI: 10.1021/acs.jpcc.9b07410
J. Phys. Chem. C 2019, 123, 28867−28880

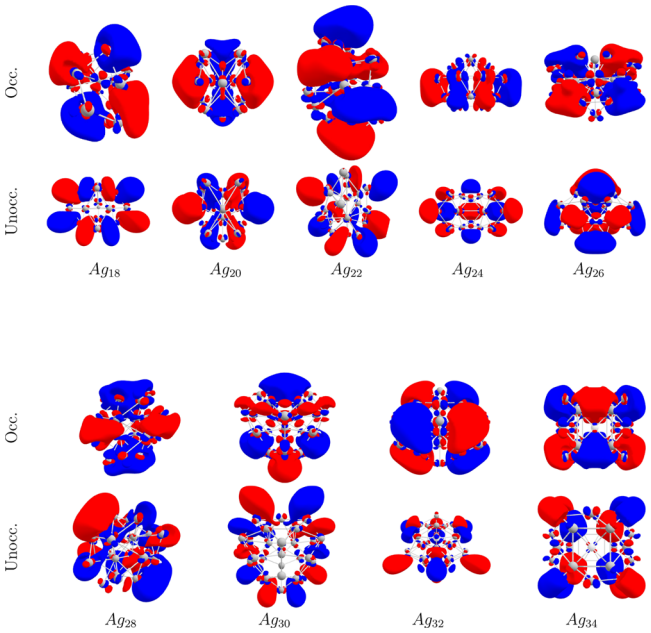

Figure 12. Doubly occupied (Occ.) and unoccupied (Unocc.) molecular orbitals pairs that correspond to the main electronic configuration of the most intensive electronic transition in the absorption spectra of Ag_n (n = 18−34) clusters calculated by the cam-B3LYP/Lanl2DZ method (the contour value of the isosurface is 0.015 au).

comparison between the theoretical end experimental spectra.[48,62−64] In this context, the different models for the frequency-dependent permittivity of silver particles look more promising for the explanation of surface and bulk plasmon resonances of real-size systems (up to 20,000 atoms within our coordination-dependent discrete interaction model that correspond to the approximate size of the spherical nanoparticles of approximately 12 nm).

APPENDIX C

Capacitance Parameter

Since there is no known connection between the capacitance parameter c and any measurable atomic quantity, this parameter should in principle be fitted as attempted by others.[20,22,27,28] We, however, found that the capacitance parameter could not be fitted from a set of spherical clusters since there was no discernible difference in the frequency-dependent polarizabilty for values in the range of 10^5 to 10^{-8} except in the region of 10 to 10^{-2} where the method showed numerical instability as shown for a 1481 atom silver cluster in Figure 13.

Due to the numerical instability from 10 to 10^{-2} and the otherwise numerical insensitivity outside this region, we have chosen to use 0.0001 au as the value of the capacitance parameter c in the fitting. It is, here, a bit surprising that the value of the capacitance parameter c does not seem to matter for clusters with only one type of atom and the exclusion of the interaction energy between fluctuating charges does not alter the polarizabilty either as seen in Figure 13. Due to the numerical instability, the polarizability can take negative values as seen for c = 1 in Figure 13, which looks more like the real part of a complex resonance.

For nanorods, we observe a similar picture though the region with numerical instability is larger and stability is only seen

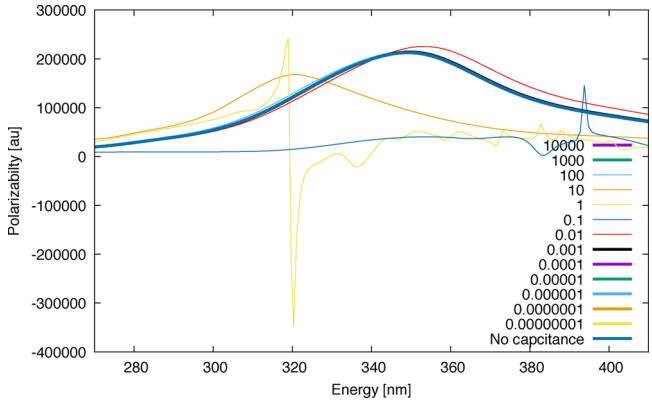

Figure 13. Polarizabilty of a 1481 atom silver cluster with different values for the capacitance parameter c. Since all curves with c = 0.001 or smaller are all on top of each other, not all curves are directly visible. For the no capacitance curve, the interaction energy between fluctuating charges has been omitted. All curves have been calculated with the fitted parameters ω_a and A.

from c = 0.001 and below (see Figure 14). While the capacitance term in eq 1 does not seem to be important for

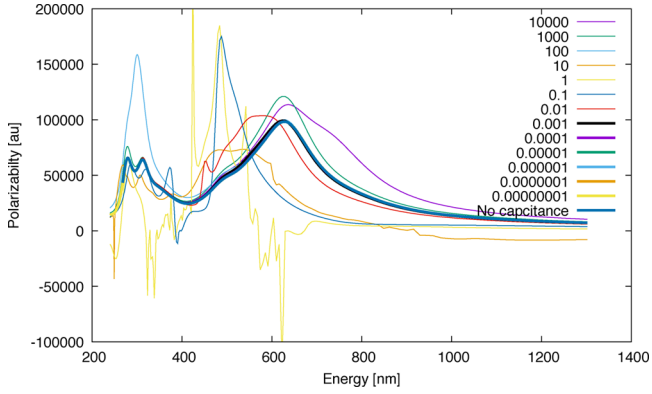

Figure 14. Polarizabilty of the Ag(6.18, 2.23) nanorod with different values for the capacitance parameter c. The values 6.18 and 2.23 are designated to the longitudinal and transverse plasmon lengths in nm, respectively. For the no capacitance curve, the interaction energy between fluctuating charges have been omitted. All curves have been calculated with the fitted parameters ω_a and A. All curves calculated with the capacitance parameter c below 0.001 or omitted are overlapping each other. The range of the polarizability for c = 1 has been cropped in order to better present the rest of the curves.

nanoclusters consisting of only one type of element, we expect it to be more important for composite materials, different close-lying metallic clusters, and clusters in external electromagnetic fields or with coordination number-dependent Gaussian charge distributions though further investigations along those lines are needed for definite conclusions.

APPENDIX D

Gamma Parameter

While the γ parameter in the Lorentzian function in eq 17 does not affect the position of the SPR, provided that γ is small in comparison to ω, the smoothing effect of γ, however, influences the absolute polarizability significantly. Since we do not fit our model to the absolute polarizability from TDDFT calculations but instead the SPR to experimental values, the γ value is instead chosen.

DOI: 10.1021/acs.jpcc.9b07410
J. Phys. Chem. C 2019, 123, 28867−28880

In Figure 15, the polarizability of a 1481 atom spherical cluster with different γ values in the 0.002−0.030 au range. In

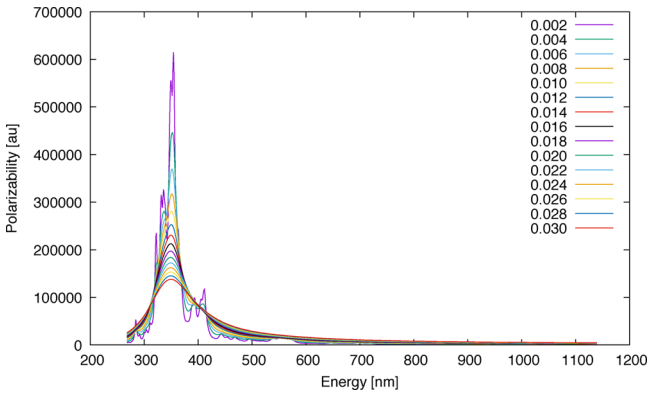

Figure 15. Polarizability of a 1481 atom spherical silver cluster with different γ values.

the 0.002−0.006 au range, several peaks are visible, and the SPR is clearly a double peak, but from approximately 0.010 au and above, the double-peak SPR becomes a smooth single peak. For the very small γ values, the SPR is therefore shifted slightly but remains constant at 0.010 au and above. Furthermore, the absolute polarizability increases more than fourfold from γ at 0.030 to 0.002 showing that γ would be a very sensitive parameter if the absolute polarizability was fitted to TDDFT calculations. While the polarizability drops, the FWHM, of course, increases significantly.

For nanorods, the effect of γ is similar to that of spheres. As seen for the Ag(6.18, 2.23) nanorod in Figure 16, the TLSPR

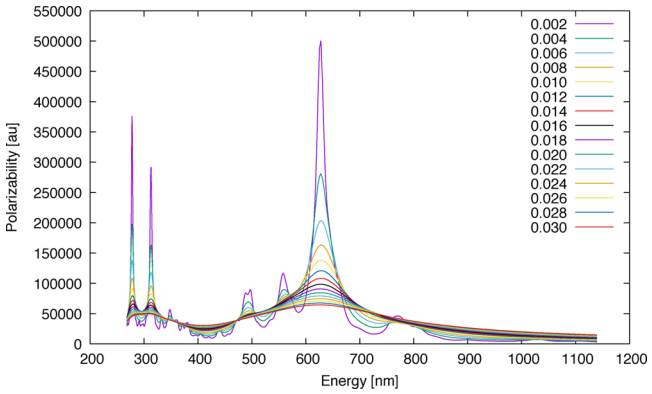

Figure 16. Polarizabilty of the Ag(6.18, 2.23) nanorod with different γ values. The values 6.18 and 2.23 are designated to the longitudinal and transverse plasmon lengths in nm, respectively.

for lower γ values is a clear double peak, while larger γ values smooth the two peaks. In order to have a γ value that still can show some structure and have a FWHM that is reasonably consistent with the experimental values from Ringe et al.,[26] we have chosen γ = 0.016 au.

While we here show absolute and not normalized polarizabilities, it is obvious that, because the γ parameter is not fitted but chosen, only the relative or normalized polarizabilities should be interpreted. We here show the absolute values in order to demonstrate how the polarizability increases with the number of atoms and the geometry of the cluster. Since the polarizability in the range tested here does not affect the position of the SPR, it is possible to later fit either a γ value or size-dependent function for γ if experimental data is found without having to fit ω_a and A again.

AUTHOR INFORMATION

Corresponding Author

*E-mail: hagren@kth.se.

ORCID

Vadim I. Zakomirnyi: 0000-0002-2049-7259
Zilvinas Rinkevicius: 0000-0003-2729-0290
Glib V. Baryshnikov: 0000-0002-0716-3385
Hans Ågren: 0000-0002-1763-9383

Notes

The authors declare no competing financial interest.

ACKNOWLEDGMENTS

H.Å. and V.I.Z. acknowledge the support of the Russian Science Foundation (project no. 18-13-00363). L.K.S. acknowledges the support of Carl Tryggers Stifetelse, project no. CTS 18-441.

REFERENCES

(1) Mie, G. Beiträge zur Optik trüber Medien, speziell kolloidaler Metallösungen. *Ann. Phys.* **1908**, *330*, 377−445.
(2) Draine, B. T.; Flatau, P. J. Discrete-Dipole Approximation For Scattering Calculations. *J. Opt. Soc. Am. A* **1994**, *11*, 1491.
(3) Waterman, P. C. Matrix formulation of electromagnetic scattering. In *Proceedings of the IEEE*; IEEE: 1965, *53*, 805−812.
(4) Yee, K. Numerical solution of initial boundary value problems involving Maxwells equations in isotropic media. In *IEEE Transactions on Antennas and Propagation*; IEEE: 1966, 302−307.
(5) Dridi, M.; Schatz, G. C. Model for describing plasmon-enhanced lasers that combines rate equations with finite-difference time-domain. *J. Opt. Soc. Am. B* **2013**, *30*, 2791.
(6) García de Abajo, F. J.; Howie, A. Retarded field calculation of electron energy loss in inhomogeneous dielectrics. *Phys. Rev. B* **2002**, *65*, 115418.
(7) Halperin, W. P. Quantum size effects in metal particles. *Rev. Mod. Phys.* **1986**, *58*, 533−606.
(8) Zakomirnyi, V. I.; Rasskazov, I. L.; Karpov, S. V.; Polyutov, S. P. New ideally absorbing Au plasmonic nanostructures for biomedical applications. *J. Quant. Spectrosc. Radiat. Transfer* **2017**, *187*, 54−61.
(9) Rasskazov, I. L.; Wang, L.; Murphy, C. J.; Bhargava, R.; Carney, P. S. Plasmon-enhanced upconversion: engineering enhancement and quenching at nano and macro scales. *Opt. Mater. Express* **2018**, *8*, 3787.
(10) Palik, E. D. *Handbook of optical constants of solids*; Academic Press: 1998.
(11) Grimme, S.; Antony, J.; Ehrlich, S.; Krieg, H. A consistent and accurate ab initio parametrization of density functional dispersion correction (DFT-D) for the 94 elements H-Pu. *J. Chem. Phys.* **2010**, *132*, 154104.
(12) Zhao; Jensen, L.; Schatz, G. C. Pyridine-$Ag_2$0 Cluster: A Model System for Studying Surface-Enhanced Raman Scattering. *J. Am. Chem. Soc.* **2006**, *128*, 2911−2919.
(13) Weissker, H.-C.; López-Lozano, X. Surface plasmons in quantum-sized noblemetal clusters: TDDFT quantum calculations and the classical picture of charge oscillations. *Phys. Chem. Chem. Phys.* **2015**, *17*, 28379−28386.
(14) Stener, M.; Nardelli, A.; De Francesco, R.; Fronzoni, G. Optical Excitations of Gold Nanoparticles: A Quantum Chemical Scalar Relativistic Time Dependent Density Functional Study. *J. Phys. Chem. C* **2007**, *111*, 11862−11871.
(15) Schira, R.; Rabilloud, F. Localized Surface Plasmon Resonance in Free Silver Nanoclusters Ag_n, n = 20-147. *J. Phys. Chem. C* **2019**, *123*, 6205−6212.

DOI: 10.1021/acs.jpcc.9b07410
J. Phys. Chem. C 2019, 123, 28867−28880

(16) Schira, R.; Rabilloud, F. Effects of Rare-Gas Matrices on the Optical Response of Silver Nanoclusters. *J. Phys. Chem. C* **2018**, *122*, 27656−27661.
(17) Gray, F. The Optical Activity of Liquids and Gases. *Phys. Rev.* **1916**, *7*, 472−488.
(18) Birge, R. R. Calculation of molecular polarizabilities using an anisotropic atom point dipole interaction model which includes the effect of electron repulsion. *J. Chem. Phys.* **1980**, *72*, 5312−5319.
(19) Thole, B. T. Molecular polarizabilities calculated with a modified dipole interaction. *Chem. Phys.* **1981**, *59*, 341−350.
(20) Jensen, L.; Åstrand, P.-O.; Sylvester-Hvid, K. O.; Mikkelsen, K. V. Frequency-Dependent Molecular Polarizability Calculated within an Interaction Model. *J. Phys. Chem. A* **2000**, *104*, 1563−1569.
(21) Jensen, L.; Schmidt, O. H.; Mikkelsen, K. V.; Åstrand, P.-O. Static and Frequency-Dependent Polarizability Tensors for Carbon Nanotubes. *J. Phys. Chem. B* **2000**, *104*, 10462−10466.
(22) Jensen, L. L.; Jensen, L. Electrostatic Interaction Model for the Calculation of the Polarizability of Large Noble Metal Nanoclusters. *J. Phys. Chem. C* **2008**, *112*, 15697−15703.
(23) Rinkevicius, Z.; Li, X.; Sandberg, J. A. R.; Mikkelsen, K. V.; Ågren, H. A hybrid density functional theory/molecular mechanics approach for linear response properties in heterogeneous environments. *J. Chem. Theory Comput.* **2014**, *10*, 989−1003.
(24) Chen, X.; Moore, J. E.; Zekarias, M.; Jensen, L. Atomistic electrodynamics simulations of bare and ligand-coated nanoparticles in the quantum size regime. *Nat. Commun.* **2015**, *6*, 8921.
(25) Jensen, L. L.; Jensen, L. Atomistic Electrodynamics Model for Optical Properties of Silver Nanoclusters. *J. Phys. Chem. C* **2009**, *113*, 15182−15190.
(26) Ringe, E.; Langille, M. R.; Sohn, K.; Zhang, J.; Huang, J.; Mirkin, C. A.; Van Duyne, R. P.; Marks, L. D. Plasmon Length: A Universal Parameter to Describe Size Effects in Gold Nanoparticles. *J. Phys. Chem. Lett.* **2012**, *3*, 1479−1483.
(27) Shanker, B.; Applequist, J. Electronic absorption spectra of molecules and aggregates with interatomic charge transfer using a normal mode treatment of the atomic monopole-dipole interaction model. *J. Chem. Phys.* **1996**, *104*, 6109−6116.
(28) Olson, M. L.; Sundberg, K. R. An atom monopole-dipole interaction model with charge transfer for the treatment of polarizabilities of π-bonded molecules. *J. Chem. Phys.* **1978**, *69*, 5400−5404.
(29) Markel, V. A. Introduction to the Maxwell Garnett approximation: tutorial. *J. Opt. Soc. Am. A* **2016**, *33*, 1244.
(30) Pyykkö, P.; Atsumi, M. Molecular single-bond covalent radii for elements 1-118. *Chem. - Eur. J.* **2009**, *15*, 186−197.
(31) Schwerdtfeger, P.; Nagle, J. K. Table of static dipole polarizabilities of the neutral elements in the periodic table. *Mol. Phys.* **2018**, *2019*, 1200−1225.
(32) Tiggesbäumker, J.; Köller, L.; Meiwes-Broer, K.-H.; Liebsch, A. Blue shift of the Mie plasma frequency in Ag clusters and particles. *Phys. Rev. A* **1993**, *48*, R1749−R1752.
(33) Scholl, J. A.; Koh, A. L.; Dionne, J. A. Quantum plasmon resonances of individual metallic nanoparticles. *Nature* **2012**, *483*, 421−427.
(34) Shao, X.; Liu, X.; Cai, W. Structural Optimization of Silver Clusters up to 80 Atoms with Gupta and Sutton-Chen Potentials. *J. Chem. Theory Comput.* **2005**, *1*, 762−768.
(35) Huang, W.; Lai, X.; Xu, R. Structural optimization of silver clusters from to using a Modified Dynamic Lattice Searching method with Constructed core. *Chem. Phys. Lett.* **2011**, *507*, 199−202.
(36) Fan, T.-E.; Shao, G.-F.; Ji, Q.-S.; Zheng, J.-W.; Liu, T.-D.; Wen, Y.-H. A multipopulations multi-strategies differential evolution algorithm for structural optimization of metal nanoclusters. *Comput. Phys. Commun.* **2016**, *208*, 64−72.
(37) Karimi, S.; Moshaii, A.; Abbasian, S.; Nikkhah, M. Surface Plasmon Resonance in Small Gold Nanoparticles: Introducing a Size-Dependent Plasma Frequency for Nanoparticles in Quantum Regime. *Plasmonics* **2019**, *14*, 851.
(38) Moroz, A. Electron Mean Free Path in a Spherical Shell Geometry. *J. Phys. Chem. C* **2008**, *112*, 10641−10652.
(39) Johnson, P. B.; Christy, R. W. Optical Constants of the Noble Metals. *Phys. Rev. B* **1972**, *6*, 4370−4379.
(40) Tzarouchis, D. C.; Ylä-Oijala, P.; Ala-Nissila, T.; Sihvola, A. Shape effects on surface plasmons in spherical, cubic, and rod-shaped silver nanoparticles. *Appl. Phys. A* **2016**, *122*, 298.
(41) Ashkarran, A. A.; Bayat, A. Surface plasmon resonance of metal nanostructures as a complementary technique for microscopic size measurement. *Int. Nano Lett.* **2013**, *3*, 50.
(42) González, A. L.; Noguez, C.; Beránek, J.; Barnard, A. S. Size, Shape, Stability, and Color of Plasmonic Silver Nanoparticles. *J. Phys. Chem. C* **2014**, *118*, 9128−9136.
(43) Slaughter, L. S.; Chang, W.-S.; Swanglap, P.; Tcherniak, A.; Khanal, B. P.; Zubarev, E. R.; Link, S. Single-Particle Spectroscopy of Gold Nanorods beyond the Quasi-Static Limit: Varying the Width at Constant Aspect Ratio. *J. Phys. Chem. C* **2010**, *114*, 4934−4938.
(44) *Gold nanorods spr vs. aspect ratio*. https://www.nanopartz.com/gold-nanoparticles-properties-nanorods-spr-aspect-ratio.asp.
(45) Jakab, A.; Rosman, C.; Khalavka, Y.; Becker, J.; Trügler, A.; Hohenester, U.; Sönnichsen, C. Highly Sensitive Plasmonic Silver Nanorods. *ACS Nano* **2011**, *5*, 6880−6885.
(46) Mayer, A. Formulation in terms of normalized propagators of a charge-dipole model enabling the calculation of the polarization properties of fullerenes and carbon nanotubes. *Phys. Rev. B* **2007**, *75*, No. 045407.
(47) Bae, G.-T.; Aikens, C. M. Time-Dependent Density Functional Theory Studies of Optical Properties of Ag Nanoparticles: Octahedra, Truncated Octahedra, and Icosahedra. *J. Phys. Chem. C* **2012**, *116*, 10356−10367.
(48) Chakraborty, I.; Govindarajan, A.; Erusappan, J.; Ghosh, A.; Pradeep, T.; Yoon, B.; Whetten, R. L.; Landman, U. The Superstable 25 kDa Monolayer Protected Silver Nanoparticle: Measurements and Interpretation as an Icosahedral $Ag_{152}(SCH_2CH_2Ph)_{60}$ Cluster. *Nano Lett.* **2012**, *12*, 5861−5866.
(49) McKee, M. L.; Samokhvalov, A. Density Functional Study of Neutral and Charged Silver Clusters Ag_n with n = 2-22. Evolution of Properties and Structure. *J. Phys. Chem. A* **2017**, *121*, 5018−5028.
(50) de Heer, W. A. The physics of simple metal clusters: experimental aspects and simple models. *Rev. Mod. Phys.* **1993**, *65*, 611−676.
(51) Yu, C.; Schira, R.; Brune, H.; von Issendorff, B.; Rabilloud, F.; Harbich, W. Optical properties of size selected neutral Ag clusters: electronic shell structures and the surface plasmon resonance. *Nanoscale* **2018**, *10*, 20821−20827.
(52) Fedrigo, S.; Harbich, W.; Buttet, J. Collective dipole oscillations in small silver clusters embedded in rare-gas matrices. *Phys. Rev. B* **1993**, *47*, 10706−10715.
(53) Runge, E.; Gross, E. K. U. Density-Functional Theory for Time-Dependent Systems. *Phys. Rev. Lett.* **1984**, *52*, 997−1000.
(54) Yanai, T.; Tew, D. P.; Handy, N. C. A new hybrid exchange-correlation functional using the Coulomb-attenuating method (CAM-B3LYP). *Chem. Phys. Lett.* **2004**, *393*, 51−57.
(55) Hay, P. J.; Wadt, W. R. Ab initio effective core potentials for molecular calculations. Potentials for the transition metal atoms Sc to Hg. *J. Chem. Phys.* **1985**, *82*, 270−283.
(56) Silverstein, D. W.; Jensen, L. Assessment of the accuracy of long-range corrected functionals for describing the electronic and optical properties of silver clusters. *J. Chem. Phys.* **2010**, *132*, 194302.
(57) Harbich, W.; Fedrigo, S.; Buttet, J. The optical absorption spectra of small Silver clusters (n=8-39) embedded in rare gas matrices. *Z. Phys. D: At., Mol. Clusters* **1993**, *26*, 138−140.
(58) Casida, M. E. Time-dependent density-functional theory for molecules and molecular solids. *J. Mol. Struct.: THEOCHEM* **2009**, *914*, 3−18.
(59) Yabana, K.; Bertsch, G. F. Time-dependent local-density approximation in real time. *Phys. Rev. B* **1996**, *54*, 4484−4487.
(60) Sinha-Roy, R.; García-González, P.; López Lozano, X.; Whetten, R. L.; Weissker, H.-C. Identifying Electronic Modes by

DOI: 10.1021/acs.jpcc.9b07410
J. Phys. Chem. C 2019, 123, 28867−28880

Fourier Transform from δ-Kick Time-Evolution TDDFT Calculations. *J. Chem. Theory Comput.* **2018**, *14*, 6417−6426.
(61) Rossi, T. P.; Kuisma, M.; Puska, M. J.; Nieminen, R. M.; Erhart, P. Kohn-Sham Decomposition in Real-Time Time-Dependent Density-Functional Theory: An Efficient Tool for Analyzing Plasmonic Excitations. *J. Chem. Theory Comput.* **2017**, *13*, 4779−4790.
(62) Udaya Bhaskara Rao, T.; Pradeep, T. Luminescent Ag_7 and Ag_8 Clusters by Interfacial Synthesis. *Angew. Chem., Int. Ed.* **2010**, *49*, 3925−3929.
(63) Rao, T. U. B.; Nataraju, B.; Pradeep, T. Ag_9 Quantum Cluster through a Solid-State Route. *J. Am. Chem. Soc.* **2010**, *132*, 16304−16307.
(64) Chakraborty, I.; Udayabhaskararao, T.; Pradeep, T. High temperature nucleation and growth of glutathione protected Ag_{75} clusters. *Chem. Commun.* **2012**, *48*, 6788.

DOI: 10.1021/acs.jpcc.9b07410
J. Phys. Chem. C 2019, 123, 28867−28880